Motile curved bacteria are Pareto-optimal

Rudi Schuech[a,1], Tatjana Hoehfurtner[a], David J. Smith[b], and Stuart Humphries[a]

[a]School of Life Sciences, Joseph Banks Laboratories, University of Lincoln, Lincoln LN6 7DL, United Kingdom; and [b]School of Mathematics, University of Birmingham, Birmingham B15 2TT, United Kingdom

Edited by Howard A. Stone, Princeton University, Princeton, NJ, and approved May 17, 2019 (received for review November 6, 2018)

Curved rods are a ubiquitous bacterial phenotype, but the fundamental question of why they are shaped this way remains unanswered. Through in silico experiments, we assessed freely swimming straight- and curved-rod bacteria of a wide diversity of equal-volume shapes parameterized by elongation and curvature, and predicted their performances in tasks likely to strongly influence overall fitness. Performance trade-offs between these tasks lead to a variety of shapes that are Pareto-optimal, including coccoids, all straight rods, and a range of curvatures. Comparison with an extensive morphological survey of motile curved-rod bacteria indicates that the vast majority of species fall within the Pareto-optimal region of morphospace. This result is consistent with evolutionary trade-offs between just three tasks: efficient swimming, chemotaxis, and low cell construction cost. We thus reveal the underlying selective pressures driving morphological diversity in a widespread component of microbial ecosystems.

motility | shape | morphology | swimming | evolution

In stark contrast to the macroscopic realm of multicellular plants and animals, in the microscopic world it remains a challenge to attribute function to any of the considerable morphological diversity that exists (1, 2). Even superficially simple traits such as the curvature of many rod-shaped bacteria have eluded evolutionary explanations, despite the ubiquity of such morphological variations. For example, while coccoids and "rods" comprise the vast majority of bacteria in the ocean, curved rods account for up to a quarter of these (3), sometimes outnumbering straight rods (4). Also observed but rarely quantified in most other habitats (5–8), curved bacteria have invested heavily in complex genetic machinery to generate and maintain their shapes (9), but we have almost no understanding of the benefits their curvature confers (1). While the biochemical and genetic mechanisms of cell growth and the maintenance of shape have received considerable attention (10–13), the costs or benefits of a particular shape have received almost none (but see refs. 14 and 15). Understanding the links between form and function is a cornerstone of modern biology, yet no studies have addressed why curvature has evolved in many bacterial clades (5–8).

The microscale physics relevant to bacteria makes addressing the physical consequences of their shapes particularly nonintuitive (16). One hypothesis is that, at microscopic scales, shape generally has no bearing on fitness (17). However, while there appears to be limited support for this "neutral morphology" theory (18), several lines of empirical evidence suggest that, just as for larger organisms, selective pressures influence microbial cell shape. Bacterial cell shape is (*i*) heritable, with some morphologies evolving independently many times; (*ii*) has high diversity, yet is typically uniform (excluding pleomorphism) within species; and (*iii*) is known to be actively modified in response to environmental changes (1).

Free-swimming cells are ubiquitous, comprise a large fraction (up to 70%) of the bacteria in the oligotrophic marine environment (19), and are part of the life cycle of many biofilm-forming species. However, the streamlining principles that explain the shapes of many swimming animals work very differently at the microscale (20). The most efficient shape for an ellipsoidal swimmer at this scale is similar to a rugby ball, but most rod-shaped bacteria are more elongated than this optimum (16). Dusenbery (16) suggests that motile bacteria are under selective pressure to elongate without bound to improve chemotactic ability, since such cells are much more resistant to random course changes imposed by Brownian motion. Hence, the diversity of elongated shapes in bacteria may well be due to evolutionary trade-offs between a number of tasks (21), such as chemotaxis and swimming efficiency. Might bacterial curvature have evolved due to similar trade-offs?

Here, we address a broad bacterial morphospace of all free-swimming curved rods, straight rods, and spheres. First, we survey the literature in search of microscopy data on curved bacteria, inserting them into a 2D parameter space of elongation and curvature to quantify their morphological diversity. In a major effort involving tens of thousands of numerical simulations, we then quantify performance throughout this morphospace in several physiologically relevant tasks likely to contribute to overall evolutionary fitness, revealing the selective advantages (and disadvantages) of curvature and elongation. Finally, from these disparate performance landscapes, we use the concept of Pareto optimality (21) to analyze the diversity of observed rod morphologies through the lens of evolutionary trade-offs between tasks. [We use the term "performance landscape" in favor of the well-known "fitness landscape" concept (22) to distinguish performance in individual tasks from overall evolutionary fitness.] While previous work (21) has approached this type of problem by leveraging abundant data on the ecology of macroscopic organisms (e.g., birds, bats, ants), such data are sparse or nonexistent at the scales relevant to bacteria. Despite this major obstacle, our direct computations of Pareto optimality allow us to identify which tasks likely constrain the evolution of shape within this morphologically diverse polyphyletic group. We thus

Significance

Bacteria exhibit a bewildering diversity of morphologies, but despite their impact on nearly all aspects of life, they are frequently classified into a few general categories, usually just "spheres" and "rods." Curved-rod bacteria are one simple variation observed in many environments, particularly the ocean. However, why so many species have evolved this shape is unknown. We show that curvature can increase swimming efficiency, revealing a widely applicable selective advantage. Furthermore, we show that the distribution of cell lengths and curvatures observed across bacteria in nature is predicted by evolutionary trade-offs between three tasks influenced by shape: efficient swimming, the ability to detect chemical gradients, and reduced cost of cell construction. We therefore reveal shape as an important component of microbial fitness.

Author contributions: R.S., D.J.S., and S.H. designed research; R.S. and T.H. performed research; R.S. and D.J.S. contributed new reagents/analytic tools; R.S. and T.H. analyzed data; and R.S. and S.H. wrote the paper.

The authors declare no conflict of interest.

This article is a PNAS Direct Submission.

[1]To whom correspondence may be addressed. Email: rudi.schuech@gmail.com.

This article contains supporting information online at www.pnas.org/lookup/suppl/doi:10.1073/pnas.1818997116/-/DCSupplemental.

Published online July 2, 2019.

link form and function at the microscale and pave the way toward a broader understanding of bacterial diversity.

Survey of Curved Bacteria Shapes

We surveyed the literature for micrographs of motile, flagellated curved-rod bacteria (*Methods*, *Survey of Observed Shapes*, and *SI Appendix*, section 1). Since a wide range of motile straight rods (from coccoids to filaments) has previously been reported (16), we included these in our subsequent calculations but focused our efforts on surveying visibly curved cells. Individual cells were segmented using MicrobeJ (23) (*Methods*, *Survey of Observed Shapes*, and *SI Appendix*, Fig. S1 and section 1) and fitted to a simple geometric model parameterized by elongation ($\mathcal{L}$) and centerline "curvature" ($\mathcal{K}$), both dimensionless and thus independent of length scale (Fig. 1, *Inset*; *Methods*, *Model Geometry*; *SI Appendix*, section 6.1). (For brevity and accessibility, instead of the typical mathematical meaning, we use the term "curvature" loosely to describe the dimensionless fraction of a full circumference formed by the cell centerline.) The survey (Fig. 1 and Dataset S3) highlights the diversity of shapes within our curved-rod parameter space: Short bean-, comma-, and long hotdog-like shapes can all be found in nature, with a few exceptionally elongated species beyond $\mathcal{L} = 10$ (*SI Appendix*, Fig. S2). Of the 11 phyla, 98 genera, and 205 species, notable members of the dataset include *Bdellovibrio* spp. (which feeds on other bacteria, including human and animal pathogens), and *Vibrio cholerae* and *V. vulnificus*, both capable of causing serious illness in humans. The median curved rod ($\mathcal{L} = 3.7$, $\mathcal{K} = 0.14$) corresponds to a rod with limited curvature (similar to *Vibrio ruber*), and 50% of all curved species fall within $\mathcal{L} = 2.3$–4.9 and $\mathcal{K} = 0.05$–0.25. There is a factor of 10 variation in diameter of an equal-volume sphere [i.e., equivalent spherical diameter (ESD)], but with no discernible correlation between size (for our purposes, ESD) and shape ($\mathcal{L}$ vs. ESD, $n = 220$, $r^2 = 0.001$, $P = 0.582$; $\mathcal{K}$ vs. ESD, $n = 220$, $r^2 = 0.005$, $P = 0.298$), we do not consider size further (*SI Appendix*, section 2). There is, however, a weak decreasing trend in curvature versus elongation ($\mathcal{L}$ vs. $\mathcal{K}$, $n = 223$, $r^2 = 0.028$, $P = 0.012$). Although toroidal bacterial morphologies do exist (*SI Appendix*, section 1), there is a conspicuous lack of motile species that are more than semicircular (Fig. 1).

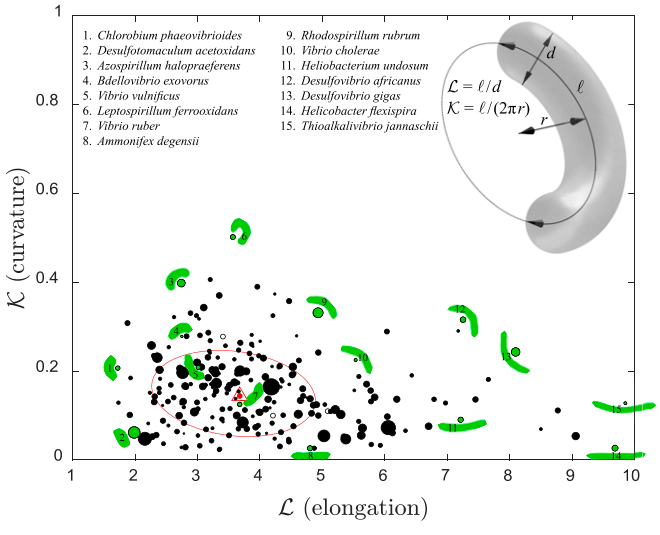

Fig. 1. Survey of extant curved-rod morphologies, with geometric parameters and definitions of dimensionless shape parameters $\mathcal{L}$ and $\mathcal{K}$ (*Inset*). The circles represent species median shapes based on segmented images, with circle radius proportional to equivalent spherical diameter (ESD) when scale data available (filled) or overall median ESD when not (open). The smallest ellipse containing 50% of all species is shown in red, and overall median species shape (and ESD) is depicted by a red filled circle, highlighted by a triangle. Silhouetted individuals (green), rescaled to constant volume, are shown for selected species (green filled circles).

Swimming Efficiency

Given that curved bacteria fill a particular region of the theoretical morphospace (Fig. 1), it is natural to ask why bacteria might be curved at all, why some are as curved as they are, and why not all conceivable curved-rod morphologies are found in nature. We first hypothesized that cell curvature might enhance the swimming speed of a bacterium, given a certain power expenditure. That is, curvature might increase Swimming Efficiency, defined as the ratio of power required to translate an equal-volume sphere to the mechanical power dissipated by the flagellar motor: $\Psi_{swim} = 6\pi\bar{a}\mu\overline{U}_{swim}^2/\overline{P}^M$, where $\bar{a}$ is equivalent cell radius (0.62 μm for all cells here), μ is dynamic viscosity of water (10^{-9} kg·s^{-1}·μm^{-1}), $\overline{U}_{swim}$ is effective swimming speed, and $\overline{P}^M$ is average power dissipated by the motor (ref. 24; *SI Appendix*, section 10.3). This hypothesis is in line with the results of Phan-Thien et al. (25), who showed that a slightly flattened triaxial ellipsoid is marginally more efficient than the best rotationally symmetric spheroid, as well as Liu et al. (26), who approximated *Caulobacter crescentus* as a straight rod with a tilted off-axis flagellum and found increased efficiency compared with the aligned case. The reason for this is a peculiarity of propulsion by a rotating flagellum—there is a trade-off between minimizing the translational resistance of the body and maximizing its rotational resistance, to reduce the power typically wasted by body counterrotation. Applied to curved rods, this idea suggests that an optimal curvature should exist, since curvature should increase both translational and rotational resistance.

Using a regularized Stokeslet Boundary Element Method (*Methods*, *Numerical Solution for Swimming Kinematics and Rotational Diffusion*, and *SI Appendix*, sections 3–9), we simulated the detailed kinematics of freely swimming curved rods propelled by rotating flagella (Fig. 2*B* and *SI Appendix*, Fig. S3 and Movie S1) over a broad theoretical morphospace spanning nearly all our observed body shapes as well as spheres, straight rods, and rings (Fig. 2*A* and *SI Appendix*, Fig. S14). All shapes were constrained to be equal volume (1 μm^3, similar to *E. coli*) to focus on variation in shape, not size, although we note that our definition of Ψ_{swim} is scale-invariant regardless. While our focus was bacterial body shape, flagellum shape also affects swimming performance. Since there is a profound scarcity of detailed data on flagellar morphology, we chose to pair each body shape with its optimal helical flagellum (i.e., optimal amplitude, wavelength, and number of wavelengths: Fig. 2*D* and *SI Appendix*, Fig. S16 and section 11.1) that maximizes Ψ_{swim} to reduce artificial biases in our results, despite this task requiring >100,000 CPU hours. We thus generated a performance landscape for Swimming Efficiency over diverse curved bacterial shapes (Fig. 3*A*).

Surprisingly, we found that over the entire morphospace, the globally optimal Swimming Efficiency is achieved not by a curved rod but a straight, slightly elongated rod comparable to a medicine capsule ($\mathcal{L} = 1.46$, $\mathcal{K} = 0$; Fig. 3*A*). However, this shape has a Swimming Efficiency advantage of just 2% over a spherical body, in general agreement with previous studies of ellipsoidal cells (16, 24, 25) (*SI Appendix*, Fig. S19), and is only 0.3% better than the semicircular curved rod located at a local maximum in the performance landscape ($\mathcal{L} = 4.0$, $\mathcal{K} = 0.70$). In fact, a diverse range of shapes exhibit essentially the same efficiency, with only long straight rods having substantially reduced performance compared with a sphere (Movie S1).

Intriguingly, the optimal curvature $\mathcal{K}$ for a given elongation $\mathcal{L}$ is approximately constant (~0.65) beyond $\mathcal{L} = 4$, with efficiencies within a few percent of that of a sphere up to $\mathcal{L} = 10$. However, even modest curvature (e.g., $\mathcal{K} = 0.2$) allows a highly elongated

straight rod ($\mathcal{L} = 10$) to mitigate its efficiency penalty by over 20%. Thus, if bacteria were to elongate for reasons other than efficient swimming, they could avoid this penalty by being curved. While Swimming Efficiency (or equivalently, speed; *SI Appendix*, section 10.3) alone cannot explain why elongated, curved bacteria have evolved, these data suggest efficiency might nonetheless apply selective pressure if it were to influence some other "higher-level" task favoring elongated cells.

Chemotactic Signal/Noise Ratio

It is commonly assumed that motile bacteria swim to enable chemotaxis (27)—the directed movement of organisms toward high concentrations of favorable compounds (e.g., nutrients) or away from unfavorable ones. To perform chemotaxis, bacteria must reliably sample chemical concentration at different points in space to determine whether the stimulus gradient is increasing or decreasing as they swim. For ellipsoidal cells, Dusenbery (16) concluded that many bacteria have likely evolved elongated shapes due to the benefits to chemotactic ability. The advantage of elongation here derives from larger resistance to random Brownian rotation—the longer a bacterium can maintain its orientation, the longer it can trust its concentration gradient estimates before Brownian motion randomizes its direction of travel. Following Dusenbery's information theory approach, we quantified how the reliability, or signal-to-noise ratio (SNR), for these gradient estimates varies with elongation $\mathcal{L}$ and curvature $\mathcal{K}$ of rod-shaped bacteria.

We note that overall chemotactic ability depends on other factors in addition to SNR. For instance, active reorientation is important and is observed as "tumbles" in *E. coli* (28) and "flicks" in *Vibrio* spp. (29). Hence, we also considered performance in a task that quantifies the effect of shape on the ability to reorient—Tumbling Ease—in which we approximate reorientations as being due to random perturbing forces, akin to Brownian motion but due to the flagella (*SI Appendix*, Figs. S9 and S10 and sections 10.4 and 10.6). In addition, since a primary purpose of chemotaxis is to maximize a cell's ability to obtain nutrients, we investigated the effect of shape on Nutrient Uptake via steady-state molecular diffusion to the cell surface (*SI Appendix*, Figs. S11 and S12 and section 10.7). However (as discussed later), we found that in contrast to chemotactic SNR, these two related tasks were unnecessary to explain the diversity of rod morphologies (*SI Appendix*, Fig. S18 and sections 12 and 13).

For a bacterium comparing concentration samples over time, Chemotactic SNR is proportional to $\Psi_{chemo} = \left(L_S\right)\left(\tau_{chemo}^{1/2}\right) = \left(\overline{U}_{chemo}^{r}\tau_{chemo}\right)\left(\tau_{chemo}^{1/2}\right) = \overline{U}_{chemo}^{r}\tau_{chemo}^{3/2}$, where L_S is the distance between samples, τ_{chemo} is the sampling time (i.e., the timescale for loss of orientation of the swimming direction), and $\overline{U}_{chemo}^{r}$ is the effective swimming speed, rescaled such that all equal-volume cells dissipate the same power (*SI Appendix*, section 10.5) (16). Chemotactic SNR will thus benefit from both increased resistance to Brownian rotation (which increases τ_{chemo}) as well as increased Swimming Efficiency $\left(\text{which increases } \overline{U}_{chemo}^{r}\right)$, so one might hypothesize that the optimal shape for Chemotactic SNR would be highly elongated as well as curved. We numerically calculated anisotropic rotational diffusivities (30) (Fig. 2*C* and *SI Appendix*, section 10.4) to quantify how τ_{chemo} varies with shape (*SI Appendix*, section 10.5.1), and calculated $\overline{U}_{chemo}^{r}$ via simulations similar to those employed for Swimming Efficiency (*SI Appendix*, section 10.5.2). Since Swimming Efficiency and Chemotactic SNR are optimized by different flagellum shapes (Fig. 2*D* and *SI Appendix*, section 10.5.2), here we again found the Ψ_{chemo}-optimized helical flagellum shape for each body shape to remove any arbitrary biases in our results (*SI Appendix*, Fig. S16 and section 11.2). Chemotactic SNR appears to increase

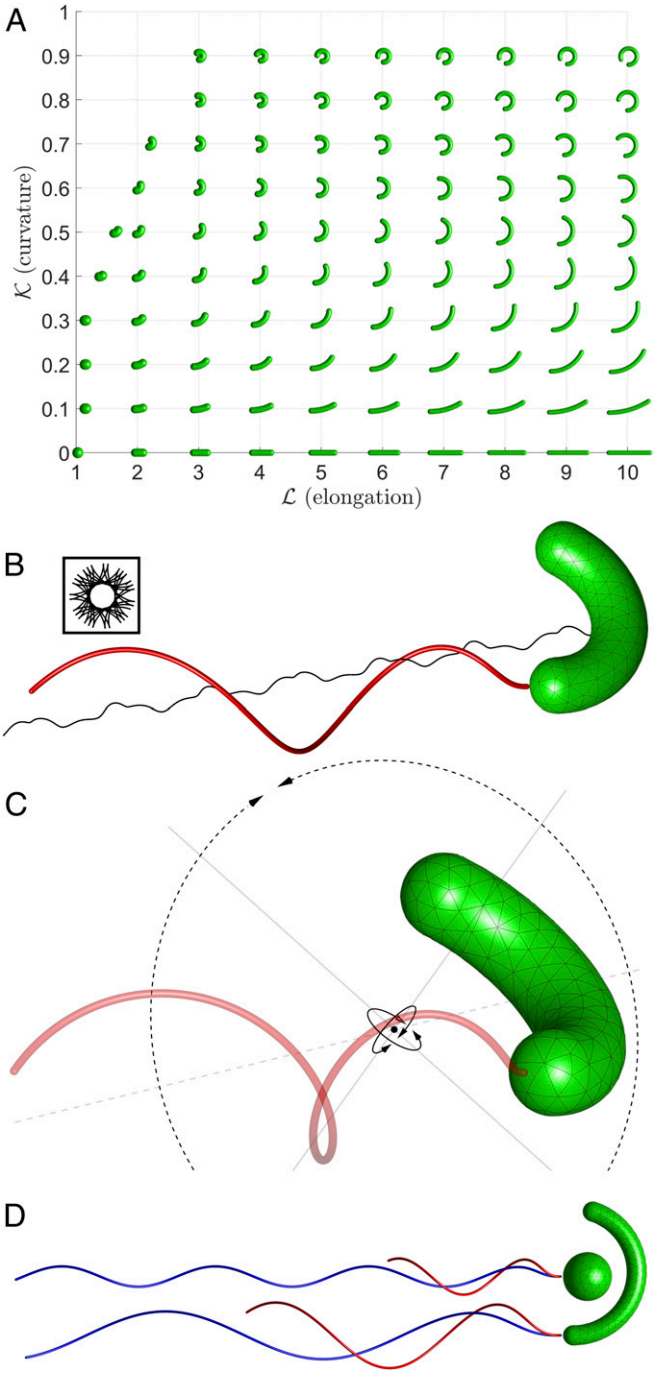

Fig. 2. (*A*) Simulated 2D morphospace of equal-volume body shapes. Empty region at upper left consists of nonphysical self-intersecting shapes. (*B*) Example body + flagellum with simulated swimming trajectory traced by the body midpoint, which appears to lack any symmetry viewed off-axis but reveals long-range rotational symmetry viewed axially (*Inset*). (*C*) The random Brownian rotation that would be superimposed onto the swimming trajectory can be quantified by three anisotropic rotational diffusivities, depicted as circles with diameter proportional to diffusivity. These rotations occur around principal axes (light gray lines) passing through the center of diffusion (black circle) (30). The largest of these (dashed) corresponds to rotations around an axis close to the flagellar axis, but it is the other two (solid) that determine how long the cell can maintain its course. (*D*) Comparison of optimal flagellar shapes for a sphere ($\mathcal{L} = 1$, $\mathcal{K} = 0$) and highly elongated curved rod ($\mathcal{L} = 10$, $\mathcal{K} = 0.5$), for Swimming Efficiency (red) and Chemotactic SNR (blue). Example second-order triangular surface meshes are shown in *B*–*D*; the flagella were similarly fully meshed (*SI Appendix*, section 5).

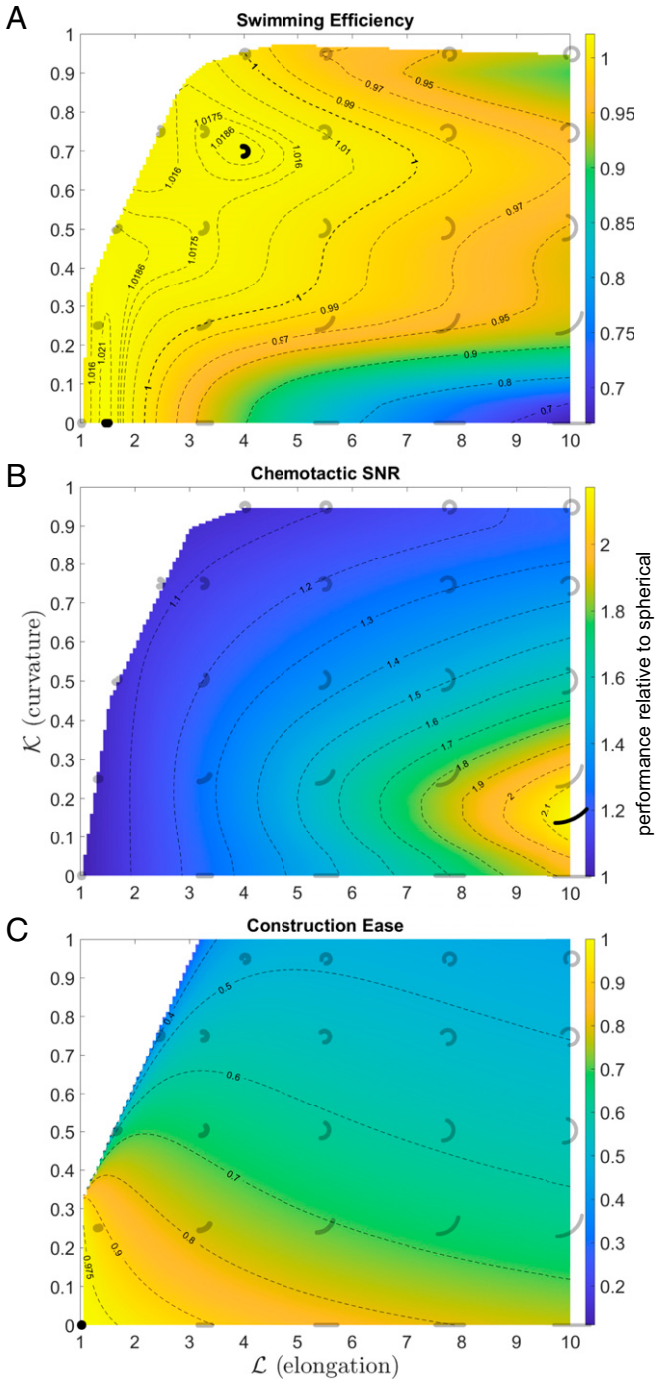

Fig. 3. Performance landscapes for putative tasks critical to curved-rod bacteria: Swimming Efficiency Ψ^n_{swim} (*A*), Chemotactic SNR Ψ^n_{chemo} (*B*), and body shape Construction Ease Ψ^n_{constr} (*C*). In each case, performance (pseudocolor and contours) is normalized relative to that of a spherical body, i.e., $\Psi^n = \Psi/\Psi_{(\mathcal{L}=1,\,\mathcal{K}=0)}$, and is thus dimensionless and scale-invariant (*SI Appendix*, section 10.2). In addition to selected shapes for reference (gray), performance maxima within our morphospace are shown (black); in *A*, these include both the global and a local maximum (see text).

without bound with flagellum length (*SI Appendix*, Fig. S15), so flagellar arclength was constrained to a maximum of 15 μm (~12 body lengths of our spherical bacterium; Fig. 2*D*) for these optimizations, consistent with observations of *E. coli* (31); however, our results are insensitive to this constraint (*SI Appendix*, section 11.2).

We find that Chemotactic SNR increases without bound with elongation (albeit slower than previous predictions; *SI Appendix*, Fig. S8) due to a faster increase in τ_{chemo} (*SI Appendix*, Fig. S6) than decrease in $\overline{U}^r_{chemo}$ (*SI Appendix*, Fig. S7) versus $\mathcal{L}$, so that there is no finite optimal cell shape for this task (Fig. 3*B*). Crucially, however, there is a nonzero optimal curvature $\mathcal{K}$ for any $\mathcal{L}$ due to another trade-off, versus $\mathcal{K}$ here, between τ_{chemo} (which favors straight rods; *SI Appendix*, Fig. S6) and $\overline{U}^r_{chemo}$ (which tends to favor substantial curvature; *SI Appendix*, Fig. S7). Thus, within our simulated morphospace, the best shape for Chemotactic SNR is a slender, slightly curved rod ($\mathcal{L} = 10$, $\mathcal{K} = 0.15$; Fig. 3*B*). Selection for Chemotactic SNR can therefore qualitatively explain why most rod-shaped bacteria are more elongated than the pill-shaped Swimming Efficiency optimum (16) as well as being curved. However, bacteria obviously cannot elongate without bound as selection solely for SNR would suggest. In addition, although we focused on surveying curved rods, many straight rods along a continuum of elongation also occur (16) and most of these presumably should not exist if the only relevant selective pressures were Swimming Efficiency and Chemotactic SNR.

Construction Ease

One reason for the existence of straight rods might be that they are simply easier to construct than curved cells. In fact, the least costly body shape is likely to be spherical (9), with specific structural proteins required to maintain both rod (32) and vibrioid or helical (33) cell shapes. It therefore seems reasonable to assume the existence of a selection pressure that penalizes morphologies with sharply curving surfaces (16, 34). While mechanochemical models of bacterial (including curved rod) cell wall growth and maintenance have been proposed (11, 35), they involve many weakly quantified parameters and a general theory of construction cost applicable to diverse morphologies is lacking. We therefore built on Dusenbery's (16) simple assumption of a minimum feasible radius of curvature, and considered geometrical cost functions (*SI Appendix*, Fig. S13 and section 10.8) based on two common metrics of surface curvature, mean and Gaussian curvature. The only cost function consistent with our observed bacterial shapes (*SI Appendix*, section 13) was based on total absolute Gaussian curvature, $\int_S |k_1 \cdot k_2|\, dA$, where k_1, k_2 are the principal curvatures at any point and S is the body surface. The absolute value causes local regions of both concave and convex surface curvature to intuitively add to total cost. Since cell membrane and wall raw materials also likely incur energetic and material costs, we then multiplied by total surface area A, taking the square root to obtain a linear scaling of total cost versus area (*SI Appendix*, section 10.8): $\text{cost} = \sqrt{A \int_S |k_1 \cdot k_2|\, dA}$. Finally, to facilitate comparison with other tasks and simplify the forthcoming analysis, we inverted the cost function to yield a Construction Ease under selective pressure to be maximized: $\Psi_{constr} = 1 \Big/ \sqrt{A \int_S |k_1 \cdot k_2|\, dA}$.

As intuitively required, the maximum Construction Ease is achieved by a coccoid cell ($\mathcal{L} = 1$, $\mathcal{K} = 0$; Fig. 3*C*), with both elongation $\mathcal{L}$ and curvature $\mathcal{K}$ generally increasing costs (*SI Appendix*, section 10.8). For almost all $\mathcal{L}$, the dependence on $\mathcal{K}$ is stronger than on $\mathcal{L}$ so that in this putative task, curvature is costlier than elongation. While total absolute Gaussian curvature is constant for all straight rods, the area penalization ensures that elongation when $\mathcal{K} = 0$ remains costly. Thus, Construction Ease should exert selective pressure on bacteria to minimize both elongation and curvature over evolutionary time.

Performance Trade-offs and Pareto Optimality

Our results quantify the relative advantages and disadvantages of bacterial curvature and elongation. Relative to straight rods of equal elongation $\mathcal{L}$ within our morphospace, curved rods of median curvature $\mathcal{K} = 0.14$ exhibit up to a 27% improvement in Swimming Efficiency and up to 12% improvement in Chemotactic SNR, but a 15–40% disadvantage in Construction Ease (Fig. 4). In reality, these performance trade-offs occur in two dimensions: A curved rod of $\mathcal{L} = 5$, $\mathcal{K} = 0.2$ will simultaneously experience pressure to straighten and shorten (to increase Construction Ease; Fig. 3*C*), to elongate (to increase Chemotactic SNR; Fig. 3*B*), and to become more curved (to increase Swimming Efficiency most rapidly; Fig. 3*A*).

Faced with such complex trade-offs between tasks, how can one approach the question of optimal shapes? The overall fitness of an organism can be assumed to be an increasing function of the performances of all tasks, but this fitness function, which depends on the relative weights of each task, is rarely known. Shoval et al. (21) discuss an elegant solution to this multiobjective optimization problem: Pareto optimality theory. This concept, borrowed from economics and engineering, delineates an optimal set of solutions that are the best trade-offs between individual tasks. In the context of this study, the Pareto optimality approach deals with the issue of unknown relative weights for each competing task by yielding a set of optimal shapes, not just a single maximizer of fitness. Within the Pareto-optimal set of solutions, it is impossible to improve at one task without sacrificing performance at another—this is an operational definition of Pareto optimality. Thus, Pareto-optimal shapes can be contrasted with suboptimal shapes that can be outperformed in all tasks simultaneously, and which are not expected to occur naturally. The shape of any given Pareto-optimal species depends on the relative contributions of each task to overall fitness in its ecological niche, i.e., the particular fitness function of that niche (21). For instance, both spherical and elongated cells might be Pareto-optimal, with the former specialized to niches favoring Construction Ease and the latter specialized to niches favoring Chemotactic SNR.

While Pareto trade-offs between a small number of critically important tasks often explain the majority of phenotypes seen in nature (21), we did not know a priori what these tasks might be for motile rod-shaped bacteria. Hence, using a simple brute-force approach based on ranking task performances across discretized morphospace (*Methods*, *Pareto Optimality and GoF*, and *SI Appendix*, section 12), we directly computed the Pareto-optimal regions resulting from the performance landscapes of many possible combinations (sets of between three and five) of our putative tasks (i.e., Swimming Efficiency, Chemotactic SNR, Construction Ease, Tumbling Ease, and Nutrient Uptake). We inferred the most likely set of crucial tasks by identifying the best goodness-of-fit (GoF) metric (*Methods*, *Pareto Optimality and GoF*, and *SI Appendix*, section 13) between each theoretically optimal set of shapes (*SI Appendix*, Fig. S18) and the morphospace region bounded by observed species (*SI Appendix*, Fig. S2 and section 1).

The best GoF corresponds to a three-way trade-off between Swimming Efficiency, Chemotactic SNR, and Construction Ease (*SI Appendix*, Fig. S18 and section 13), indicating that these three tasks have been critically important in shaping the evolution of motile curved rods. The resulting Pareto-optimal region (Fig. 5 and *SI Appendix*, section 12) reproduces the decreasing trend in maximum curvature $\mathcal{K}$ of observed morphologies and encompasses the diversity of species shapes, with most bacteria apparently employing a generalist strategy but some species specializing in just one or two tasks. In particular, the boundaries (i.e., fronts) of the main Pareto-optimal region consist of bacteria engaged in trade-offs between only two tasks: Construction Ease versus Chemotactic SNR for most straight rods along the elongation ($\mathcal{L}$) axis (e.g., *Ammonifex degensii*),

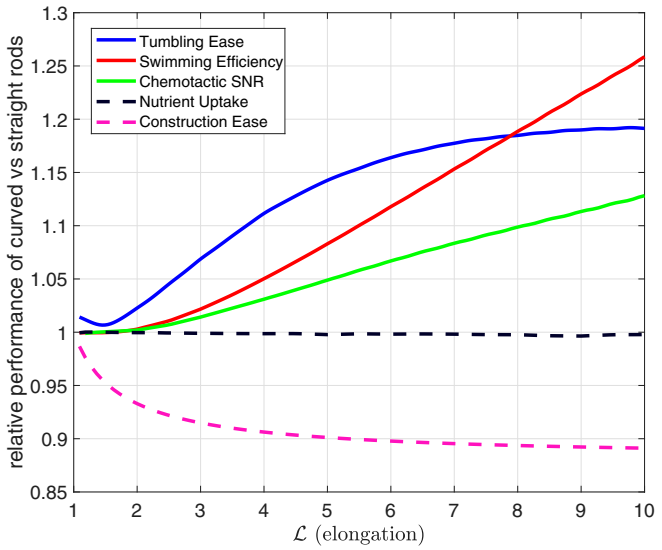

Fig. 4. Ratio of performance of curved ($\mathcal{K} = 0.14$, i.e., the species median) to straight ($\mathcal{K} = 0$) rods at different tasks, calculated by evaluating the interpolants for each task (Fig. 3 and *SI Appendix*, Figs. S10 and S12 and section 10.1) along these transects. Some tasks are improved by curvature (solid lines), while others become worse (dashed lines).

and Swimming Efficiency versus Chemotactic SNR along most of the upper boundary (e.g., *Rhodospirillum rubrum*). There are only two theoretically suboptimal outliers: *Desulfovibrio africanus* ($\mathcal{L} = 7.3$, $\mathcal{K} = 0.32$), and *Leptospirillum ferrooxidans* ($\mathcal{L} = 3.6$, $\mathcal{K} = 0.50$), which often has an extreme C-shape and erodes ferrite surfaces (36), possibly facilitating high contact area with its substrate.

Crucially, the Pareto-optimal region excludes almost all shapes that are not seen in nature, e.g., short, sharply curved cells and motile ring-shaped cells. However, we note the conspicuous presence of a small "evolutionary island" of semicircular rods due to the nearby relative maximum in the Swimming Efficiency performance landscape (Fig. 3*A*). While these shapes may be theoretically optimal, their absence in nature (at least from our survey) could simply be a consequence of the vast "sea" of suboptimality isolating them from observed morphologies. We also predict, but do not observe, the existence of highly elongated, moderately curved rods (e.g., $\mathcal{L} = 10$, $\mathcal{K} = 0.3$). However, in reality, all curved-rod bacteria may have a 3D helical shape that is difficult to discern from typical microscopy images (37). We suspect that the likelihood of cell curvature appearing clearly helical and not planar increases with $\mathcal{L}$, so that such long, curved rods do exist in a sense, but are helically shaped and beyond the scope of this study.

Discussion

We first performed a thorough survey of literature containing micrographs of curved bacteria to quantify extant morphologies (Fig. 1), although we note that selection bias and other sources of error may exist in published images as well as our analysis of them, despite our efforts to minimize the latter (*SI Appendix*, section 1). We then modeled performance in several putative tasks likely to be important to motile bacteria, in some cases with little a priori knowledge of which morphologies might optimize them. Faced with substantial uncertainties and variability in flagellar morphology across species (38), we eliminated arbitrary biases in our results by finding the optimal flagellum for each body shape, separately for both efficient swimming and chemotaxis (*SI Appendix*, Fig. S16 and section 11). Our detailed numerical simulations (Fig. 2 and *SI Appendix*, sections 3–11) reveal performance landscapes with complex topography [i.e., nonelliptical

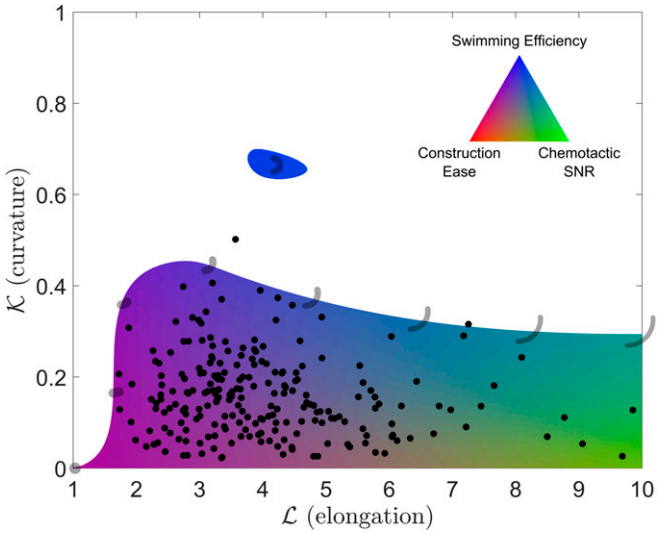

Fig. 5. Pareto-optimal curved-rod morphologies. Colored regions represent the set of shapes that are Pareto-optimal resulting from trade-offs between Swimming Efficiency, Chemotactic SNR, and Construction Ease; white region represents suboptimal shapes; and dots represent observed species medians. Selected simulated morphologies are plotted along the main optimal/suboptimal Pareto front as well as at the centroid of the disconnected Pareto-optimal "island." RGB color values were assigned by normalizing performances in each task within the optimal region between 0 and 1. Color thus signifies relative, not absolute, trade-offs between tasks as indicated by the color triangle (*Inset*). Not all colors in the triangle are realized because not all possible trade-offs are realized (e.g., the shapes that excel at Construction Ease also excel at Swimming Efficiency).

contours (Fig. 3 *A* and *C*), local maxima (Fig. 3*A*), nonfinite optimal shapes (Fig. 3*B*)], which combine to yield a Pareto-optimal region that is not a simple triangle (Fig. 5) as would be expected under simplifying assumptions (21) (*SI Appendix*, section 12). By considering many combinations of the putative tasks in our analysis of Pareto optimality (*SI Appendix*, section 12), we gain confidence (*SI Appendix*, section 13) in our conclusion that the tasks constraining evolution of curved morphologies are Swimming Efficiency, Chemotactic SNR, and Construction Ease. While we cannot rule out the importance of additional tasks such as navigation through viscoelastic gels (15), avoidance of predation (39), attachment or detachment from surfaces (14, 40), and activities related to life in biofilms (41), our proposed set of three tasks is minimally complex in the sense that this is the minimum number required to explain the diversity of observed morphologies (*SI Appendix*, section 12).

The inclusion of Swimming Efficiency in the small set of critically important tasks shaping the evolution of curved bacteria might seem surprising given the ranges of variation seen in the performance landscapes: Construction Ease and Chemotactic SNR display relatively strong effects of shape, with factors of 3 and 2.2 variation, respectively, over the Pareto-optimal region of morphospace (Fig. 3 *B* and *C*). Although Swimming Efficiency exhibits a factor of 1.5 variation overall, there is far less variability (i.e., 10%) over the majority of considered shapes, particularly those that determine the upper front of the main Pareto-optimal region (Figs. 3*A* and 5). This observation highlights a core difficulty with the evolutionary multiobjective optimization problem—the relative contributions of each task to overall fitness are unknown, so that slight changes in traits such as Swimming Efficiency may have a disproportionately large impact on fitness (42). Furthermore, natural selection operates primarily on tiny variations in fitness that are difficult or impossible to observe experimentally (43). Last, Swimming Efficiency is a fundamental motility parameter and is likely to contribute to many other higher-level tasks, so its effect on overall fitness is probably compounded. For instance, not only is Chemotactic SNR enhanced by curvature due to its dependence on Swimming Efficiency, but overall chemotactic ability will depend on how quickly the cell can swim toward better conditions, in addition to the reliability of its gradient measurements. Experiments with marine bacteria, which tend to be fast-swimming but live in a nutrient-poor environment, have confirmed a strong relationship between swimming speed and overall chemotactic ability (44). Nonetheless, it is possible that our Pareto optimality approach, due to its insensitivity to absolute performance differences (*SI Appendix*, section 12), could lead to overinterpretation of the importance of tasks like Swimming Efficiency that seem to exhibit small variations across morphospace. Further experimental work, especially quantification of flagellar morphologies and swimming kinematics, is warranted to further inform efforts in this field.

The diversity of bacterial morphologies found in nature is reminiscent of the perhaps even larger diversity in marine phytoplankton, which prompted the "the paradox of the plankton" posed by Hutchinson (45). The paradox asked how there can be such a wide range of phytoplankton species, all competing for the same resources in the same habitat, despite the competitive exclusion principle predicting that one species should eventually outcompete the rest. Many resolutions of the paradox note that the open ocean is not a homogeneous habitat as originally thought, but quite spatially and temporally complex at small scales, so that species actually occupy different ecological niches (46). Similarly, while the diversity of bacterial morphologies coexisting in environments such as biofilms (47) or the human gut (48) might seem paradoxical, this level of habitat classification is far too coarse to be relevant to bacteria. In contrast to macroscopic organisms (49), our understanding of the niches occupied by bacteria is extremely limited. Nonetheless, our results provide testable predictions for which tasks, and perhaps microniches, different rod-shaped morphologies are specialized. For example, highly elongated species should display very effective chemotaxis and therefore might be adapted to habitats with shallow nutrient gradients. Species with high curvature, being efficient swimmers, might tend to live in oligotrophic or highly viscous environments—for instance, while seawater is of low viscosity on average, there is mounting evidence of significant spatial and temporal variation due to phytoplankton exudates and other factors (50). The low cost of construction we predict for nearly spherical bacteria is difficult to observe, but one might speculate a correlation between ease of construction and growth rate. While controlling for the many confounding factors that vary across species is challenging, we anticipate that advances in experimental (51) and phylogenetic methods (52) will enable direct tests of these predictions.

Methods

Survey of Observed Shapes. We examined all images in Bergey's *Manual of Systematic Bacteriology* (5–9) and *The Prokaryotes* (53) for curved rods. We additionally filtered an in-house manually collected dataset of bacterial morphologies compiled according to the methods of ref. 54 for all species that were reported as "curved," "slightly curved," "bent," "kidney-shaped," "crescent-shaped," "comma-shaped," "crooked," "C-shaped," or "boat-shaped." We then searched for these species (via genus) on http://www.bacterio.net/ and scanned the publications listed there for images of cells; if this failed, we tried a Google Scholar search for publications on the species. We restricted our searches to bacteria identified to species level, known or likely to exhibit swimming motility (i.e., flagellated, or swimming motility demonstrated for all other members of genus), and to images that contained at least some perceptibly curved individuals (see *SI Appendix*, section 1, for full details of the methodology). In all, our dataset consists of 4,903 individual bacteria across 363 images (Dataset S2).

Our morphology measures (elongation $\mathcal{L}$ and curvature $\mathcal{K}$) were determined after semiautomatically segmenting the cells using the "Rod-Shaped" shape

type in MicrobeJ (23) (*SI Appendix*, Fig. S1 and section 1). Each segmented image was manually inspected to ensure accuracy of all measurements.

We computed unweighted species medians of $\mathcal{L}$, $\mathcal{K}$, and equivalent spherical diameter by first taking medians within each image, aggregating multiple images into one dataset for this purpose when they were stated to represent identical conditions (e.g., strain, substrate, nutrient conditions, etc.). We then calculated the medians of these values across all images found for each species, regardless of strain (Dataset S3). Using means instead of medians yielded similar results and did not affect our conclusions.

To calculate GoF between the theoretically Pareto-optimal regions and observed bacterial shapes, we computed a polygonal boundary similar to a convex hull around the latter data points (*SI Appendix*, Fig. S2; see *SI Appendix*, section 1 for more details).

Model Geometry. The bacterial cell body was modeled as a curved rod of circular cross section with hemispherical caps on both ends. It has been suggested that all curved-rod bacteria are actually short sections of a 3D helix (37), but for simplicity we assume that the cell centerline always lies in a plane. All cells had a constant, arbitrary (*SI Appendix*, section 6.1) volume of 1 μm^3, so each body shape was determined by two dimensionless aspect ratios: $\mathcal{L}=\ell/d$, which describes elongation, and $\mathcal{K}=\ell/(2\pi r)$, which describes the degree of centerline curvature of the curved rod shape, where ℓ is the total arclength of the body centerline (from pole to pole), d is the body diameter, and r is the radius of curvature of the body centerline (Fig. 1, *Inset*).

The flagellum was modeled as a modified right-handed helix of finite circular cross section (radius, 0.03 μm) parameterized by amplitude a, wavelength λ, and number of wavelengths n_λ, as in Shum et al. (24) (*SI Appendix*, section 6.2). The flagellum axis was aligned with the cell centerline at the rear body pole for simplicity (Fig. 2 *B–D* and *SI Appendix*, Fig. S3). However, we note that there is considerable uncertainty as to the orientation in real cells; we briefly tested an alternative orientation of the flagellum (*SI Appendix*, section 6.2 and Fig. S4) but found that it resulted in inferior Swimming Efficiency for all body shapes (*SI Appendix*, section 11.1 and Fig. S17).

Numerical Solution for Swimming Kinematics and Rotational Diffusion. A regularized Stokeslet Boundary Element Method (*SI Appendix*, sections 3 and 4) was used to numerically solve for the inertialess kinematics (*SI Appendix*, Fig. S5) of freely swimming cells (*SI Appendix*, sections 7 and 8) propelled by a rotating flagellum in water, i.e., their effective swimming speed $\overline{U}_{swim}$ and average power dissipation by the flagellar motor $\overline{P}^M$. This type of numerical method has been used extensively to model swimming microorganisms; our approach generally follows that of Smith (55) with several performance improvements detailed in *SI Appendix*, section 5. We also used this code to quantify the anisotropic Brownian diffusion (30) of curved-rod bacteria, accounting for the stabilizing effect of the flagellum in the case of Chemotactic SNR (56) (*SI Appendix*, section 10.4). Specifically, we calculated the timescale for loss of orientation τ, which depends on the rotational diffusion coefficients for rotations around the two principal axes normal to the swimming direction (16) (Fig. 2*C* and *SI Appendix*, sections 10.5.1 and 10.6.1).

Pareto Optimality and GoF. For each putative set of evolutionarily crucial tasks (out of 38 combinations), we sampled the interpolant of each task's performance landscape throughout a discretized grid of 125 × 100 points in morphospace, and removed the dominated points, which are beaten at all tasks by at least one other point (full details in *SI Appendix*, section 12). For each set of tasks, we computed Hargrove et al.'s (57) GoF parameter between the resulting Pareto-optimal region of morphospace and the boundary around observed species shapes as $\text{GoF}=[R_C/(R_B+R_C)][R_C/(R_A+R_C)]$, where R_A is the area within the observations but outside the optimal region, R_B is the area within the optimal region but outside the observations, and R_C is the area shared by both the observations and optimal region (*SI Appendix*, Fig. S18 and section 13).

Code Availability. The computer code used in this work is available at https://github.com/rschuech/RSBEM under the GPL 3.0 license; note that it is under active development.

Data Availability Statement. The relevant data supporting the findings of this study are available as supplementary data (Datasets S2 and S3).

ACKNOWLEDGMENTS. R.S. and S.H. were supported by Grant RL-2012-022 from the Leverhulme Trust.

1. K. D. Young, The selective value of bacterial shape. *Microbiol. Mol. Biol. Rev.* **70**, 660–703 (2006).
2. D. T. Kysela, A. M. Randich, P. D. Caccamo, Y. V. Brun, Diversity takes shape: Understanding the mechanistic and adaptive basis of bacterial morphology. *PLoS Biol.* **14**, e1002565 (2016).
3. R. La Ferla *et al*., Are prokaryotic cell shape and size suitable to ecosystem characterization? *Hydrobiologia* **726**, 65–80 (2014).
4. F. J. Jochem, Morphology and DNA content of bacterioplankton in the northern Gulf of Mexico: Analysis by epifluorescence microscopy and flow cytometry. *Aquat. Microb. Ecol.* **25**, 179–194 (2001).
5. G. M. Garrity, D. R. Boone, R. W. Castenholz, Eds., *Bergey's Manual of Systematic Bacteriology* (Springer-Verlag, New York, NY, ed. 2, 2001), vol. 1.
6. D. J. Brenner, N. R. Krieg, J. T. Staley, G. M. Garrity, Eds. *Bergey's Manual of Systematic Bacteriology* (Springer-Verlag, New York, NY, ed. 2, 2005), vol. 2, parts A, B, and C.
7. P. Vos *et al*., Eds., *Bergey's Manual of Systematic Bacteriology* (Springer-Verlag, New York, NY, ed. 2, 2009), vol. 3.
8. N. R. Krieg *et al*., Eds., *Bergey's Manual of Systematic Bacteriology* (Springer-Verlag, New York, NY, ed. 2, 2010), vol. 4.
9. W. B. Whitman *et al*., *Bergey's Manual of Systematic Bacteriology* (Springer-Verlag, New York, NY, ed. 5, 2012), vol. 5, parts A and B.
10. K. S. Cannon, B. L. Woods, A. S. Gladfelter, The unsolved problem of how cells sense micron-scale curvature. *Trends Biochem. Sci.* **42**, 961–976 (2017).
11. S. Banerjee, N. F. Scherer, A. R. Dinner, Shape dynamics of growing cell walls. *Soft Matter* **12**, 3442–3450 (2016).
12. J. S. Kim, S. X. Sun, Morphology of *Caulobacter crescentus* and the mechanical role of crescentin. *Biophys. J.* **96**, L47–L49 (2009).
13. C. S. Wright *et al*., Intergenerational continuity of cell shape dynamics in *Caulobacter crescentus*. *Sci. Rep.* **5**, 9155 (2015).
14. A. Persat, H. A. Stone, Z. Gitai, The curved shape of *Caulobacter crescentus* enhances surface colonization in flow. *Nat. Commun.* **5**, 3824 (2014).
15. T. M. Bartlett *et al*., A periplasmic polymer curves *Vibrio cholerae* and promotes pathogenesis. *Cell* **168**, 172–185.e15 (2017).
16. D. B. Dusenbery, *Living at Micro Scale: The Unexpected Physics of Being Small* (Harvard University Press, Cambridge, MA, 2011).
17. J. T. Bonner, *Randomness in Evolution* (Princeton University Press, London, ed. 1, 2013).
18. D. J. G. Lahr, H. D. Laughinghouse, 4th, A. M. Oliverio, F. Gao, L. A. Katz, How discordant morphological and molecular evolution among microorganisms can revise our notions of biodiversity on Earth. *BioEssays* **36**, 950–959 (2014).
19. H.-P. Grossart, L. Riemann, F. Azam, Bacterial motility in the sea and its ecological implications. *Aquat. Microb. Ecol.* **25**, 247–258 (2001).
20. S. Vogel, *Life in Moving Fluids: The Physical Biology of Flow* (Princeton University Press, 1994).
21. O. Shoval *et al*., Evolutionary trade-offs, Pareto optimality, and the geometry of phenotype space. *Science* **336**, 1157–1160 (2012).
22. G. R. McGhee, *The Geometry of Evolution* (Cambridge Core, 2006).
23. A. Ducret, E. M. Quardokus, Y. V. Brun, MicrobeJ, a tool for high throughput bacterial cell detection and quantitative analysis. *Nat. Microbiol.* **1**, 16077 (2016).
24. H. Shum, E. A. Gaffney, D. J. Smith, Modelling bacterial behaviour close to a no-slip plane boundary: The influence of bacterial geometry. *Proc. R. Soc. A Math. Phys. Eng. Sci.* **466**, 1725–1748 (2010).
25. N. Phan-Thien, T. Tran-Cong, M. Ramia, A boundary-element analysis of flagellar propulsion. *J. Fluid Mech.* **184**, 533–549 (1987).
26. B. Liu *et al*., Helical motion of the cell body enhances *Caulobacter crescentus* motility. *Proc. Natl. Acad. Sci. U.S.A.* **111**, 11252–11256 (2014).
27. G. H. Wadhams, J. P. Armitage, Making sense of it all: Bacterial chemotaxis. *Nat. Rev. Mol. Cell Biol.* **5**, 1024–1037 (2004).
28. H. C. Berg (1993) *Random Walks in Biology* (Princeton University Press, Princeton, NJ).
29. R. Stocker, J. R. Seymour, Ecology and physics of bacterial chemotaxis in the ocean. *Microbiol. Mol. Biol. Rev.* **76**, 792–812 (2012).
30. W. A. Wegener, Diffusion coefficients for rigid macromolecules with irregular shapes that allow rotational-translational coupling. *Biopolymers* **20**, 303–326 (1981).
31. L. Turner, A. S. Stern, H. C. Berg, Growth of flagellar filaments of *Escherichia coli* is independent of filament length. *J. Bacteriol.* **194**, 2437–2442 (2012).
32. N. Iwai, K. Nagai, M. Wachi, Novel *S*-benzylisothiourea compound that induces spherical cells in *Escherichia coli* probably by acting on a rod-shape-determining protein(s) other than penicillin-binding protein 2. *Biosci. Biotechnol. Biochem.* **66**, 2658–2662 (2002).
33. N. Ausmees, J. R. Kuhn, C. Jacobs-Wagner, The bacterial cytoskeleton: An intermediate filament-like function in cell shape. *Cell* **115**, 705–713 (2003).
34. A. L. Koch, What size should a bacterium be? A question of scale. *Annu. Rev. Microbiol.* **50**, 317–348 (1996).
35. H. Jiang, S. X. Sun, Growth of curved and helical bacterial cells. *Soft Matter* **8**, 7446–7451 (2012).
36. J. A. Rojas-Chapana, H. Tributsch, Interfacial activity and leaching patterns of *Leptospirillum ferrooxidans* on pyrite. *FEMS Microbiol. Ecol.* **47**, 19–29 (2004).
37. S. Cooper, Helical growth and the curved shape of *Vibrio cholerae*. *FEMS Microbiol. Lett.* **198**, 123–124 (2001).
38. C. Brennen, H. Winet, Fluid mechanics of propulsion by cilia and flagella. *Annu. Rev. Fluid Mech.* **9**, 339–398 (1977).

39. K. R. Conley, K. R. Sutherland, Particle shape impacts export and fate in the ocean through interactions with the globally abundant appendicularian *Oikopleura dioica*. *PLoS One* **12**, e0183105 (2017).
40. R. R. Bennett *et al*., Species-dependent hydrodynamics of flagellum-tethered bacteria in early biofilm development. *J. R. Soc. Interface* **13**, 20150966 (2016).
41. W. P. J. Smith *et al*., Cell morphology drives spatial patterning in microbial communities. *Proc. Natl. Acad. Sci. U.S.A.* **114**, E280–E286 (2017).
42. R. E. Lenski, M. R. Rose, S. C. Simpson, S. C. Tadler, Long-term experimental evolution in *Escherichia coli*. I. Adaptation and divergence during 2,000 generations. *Am. Nat.* **138**, 1315–1341 (1991).
43. R. C. Lewontin, *The Genetic Basis of Evolutionary Change* (Columbia University Press, New York, 1974).
44. K. Son, F. Menolascina, R. Stocker, Speed-dependent chemotactic precision in marine bacteria. *Proc. Natl. Acad. Sci. U.S.A.* **113**, 8624–8629 (2016).
45. G. E. Hutchinson, The paradox of the plankton. *Am. Nat.* **95**, 137–145 (1961).
46. S. Roy, J. Chattopadhyay, Towards a resolution of "the paradox of the plankton": A brief overview of the proposed mechanisms. *Ecol. Complex.* **4**, 26–33 (2007).
47. F. B. Dazzo, K. J. Klemmer, R. Chandler, Y. G. Yanni, In situ ecophysiology of microbial biofilm communities analyzed by CMEIAS computer-assisted microscopy at single-cell resolution. *Diversity* **5**, 426–460 (2013).
48. L. E. Martínez *et al*., *Helicobacter pylori* strains vary cell shape and flagellum number to maintain robust motility in viscous environments. *Mol. Microbiol.* **99**, 88–110 (2016).
49. H. Sheftel, O. Shoval, A. Mayo, U. Alon, The geometry of the Pareto front in biological phenotype space. *Ecol. Evol.* **3**, 1471–1483 (2013).
50. I. R. Jenkinson, X. X. Sun, L. Seuront, Thalassorheology, organic matter and plankton: Towards a more viscous approach in plankton ecology. *J. Plankton Res.* **37**, 1100–1109 (2015).
51. S. Takeuchi, W. R. DiLuzio, D. B. Weibel, G. M. Whitesides, Controlling the shape of filamentous cells of *Escherichia coli*. *Nano Lett.* **5**, 1819–1823 (2005).
52. M. Pagel, A. Meade, BayesTraits Version 3.0.1. (2007). http://www.evolution.rdg.ac.uk/BayesTraits.html. Accessed 17 June 2019.
53. M. P. Starr, H. Stolp, H. G. Trüper, A. Balows, H. G. Schlegel, Eds., *The Prokaryotes* (Springer, Berlin, 1981).
54. F. E. Baidouri, C. Venditti, S. Humphries, Independent evolution of shape and motility allows evolutionary flexibility in Firmicutes bacteria. *Nat. Ecol. Evol.* **1**, 0009 (2017).
55. D. J. Smith, A boundary element regularised Stokeslet method applied to cilia and flagella-driven flow. *Proc. R. Soc. A Math. Phys. Eng. Sci.* **465**, 3605–3626 (2009).
56. J. G. Mitchell, The energetics and scaling of search strategies in bacteria. *Am. Nat.* **160**, 727–740 (2002).
57. W. W. Hargrove, F. M. Hoffman, P. F. Hessburg, Mapcurves: A quantitative method for comparing categorical maps. *J. Geogr. Syst.* **8**, 187–208 (2006).